

1 Satellite observations of the small-scale cyclonic eddies in the western

2 South China Sea

3 Fenfen Liu¹, Shilin Tang^{2,*}, and Chuqun Chen²

4 ¹ School of Marine Sciences, Sun Yat-sen University, Guangzhou 510006, China

5 ² State Key Laboratory of Tropical Oceanography, South China Sea Institute of
6 Oceanology, Chinese Academy of Sciences, Guangzhou 510301, China

7 * Corresponding author: Shilin Tang, State Key Laboratory of Tropical Oceanography,
8 South China Sea Institute of Oceanology, Chinese Academy of Sciences, Guangzhou
9 510301, China. (sltang2009@gmail.com)

10

11

12

13

14

15

16

17

18

19 **Abstract**

20 High-resolution ocean color observation offers an opportunity to investigate the
21 oceanic small-scale processes. In this study, The Medium Resolution Imaging
22 Spectrometer (MERIS) daily 300-m data are used to study small-scale processes in
23 the western South China Sea. It is indicated that the cyclonic eddies with horizontal
24 scales of 10 km are frequently observed during upwelling season of each year over
25 2004-2009. These small-scale eddies are generated in the vicinity of the southern
26 front of the cold tongue, and then propagate eastward with a speed of approximately
27 12 cm s^{-1} . This propagation speed is consistent with the velocity of the western
28 boundary current. As a result, the small-scale eddies keep rotating high levels of the
29 phytoplankton away from the coastal areas, resulting in the accumulation of
30 phytoplankton in the interior of the eddies. The generation of the small-scale eddies
31 may be associated with strengthening of the relative movement between the rotation
32 speed of the anticyclonic mesoscale eddies and the offshore transport. With the
33 increases of the normalized rotation speed of the anticyclonic mesoscale eddies
34 relative to the offshore transport, the offshore current become meander under the
35 impacts of the anticyclonic mesoscale eddies. The meandered cold tongue and
36 instability front may stimulate the generation of the small-scale eddies. Unidirectional
37 uniform wind along cold tongue may also contribute to the formation of the
38 small-scale eddies.

39

40

42 1. Introduction

43 Approximately 90% of the kinetic energy of ocean circulation is contained in
44 small-scale features, and 50% of the vertical exchange of water mass properties
45 between the upper and the deep ocean may occur at the submesoscale and mesoscale
46 (Bouffard et al., 2012). Mesoscale eddies with horizontal scales of 50-500 km can be
47 observed using altimeters. However, the smaller scale eddies (with horizontal scales
48 below 50 km) cannot be resolved by conventional altimeters (Liu et al., 2008).
49 Satellite ocean color sensors provide high-quality observations of the bio-optical
50 constitute at a spatial resolution better than altimeters. The spatial resolutions of most
51 ocean color satellites fall in the range of 300 m to 1.1 km (at nadir viewing). The
52 high-resolution bio-optical observations reveal more details of small-scale
53 phytoplankton structures. By tracking these small-scale biological features, one can
54 determine the circulation pattern if the motion speed is large with respect of the
55 growth and grazing of the phytoplankton (Pegau et al., 2002). Recently, the Medium
56 Resolution Imaging Spectrometer (MERIS) full-resolution (FR, 300 m) data set is
57 available publicly. The MERIS FR (300 m) phytoplankton fields are rich in smaller
58 scale biological features and provide opportunities to study the small-scale processes.
59 Generally, the time period of the small-scale ocean variability ranges from several
60 days to several weeks. However, the widely used ocean color data are usually
61 averaged into weekly or monthly products in order to obtain a large spatial coverage.
62 This time-averaging may smooth the phytoplankton variability on day-scale (Genin
63 and Boehlert, 1985). Therefore, the study of the small-scale processes requires higher
64 space-time resolution of ocean color observation.

65 The South China Sea (SCS) is the largest marginal basin within the western
66 Pacific, with a total area of 3.5 million km² and a basin depth of > 3000 m (0°–25°N,
67 100°–125°E, figure 1). The SCS is oligotrophic with limited nitrogen and phosphorus
68 within the euphotic layer. A high abundance of phytoplankton mainly occurs in the
69 Gulf of Tonkin, the western South China Sea (SCS) and the Sunda Shelf in summer
70 (Ning et al., 2004). It was reported that a phytoplankton filament in the western SCS
71 is consistent with the mesoscale eddies transportation and Ekman upwelling (Tang et
72 al., 2004; Xie et al., 2003; Xiu and Chai, 2011). However, there have been only
73 limited studies on the small-scale process and its phytoplankton footprints (Nicholson,
74 2012). In this study, the daily MERIS FR data are used to identify the phytoplankton
75 variability associated with the small-scale dynamic processes. In this paper, we call
76 eddies with diameters smaller than 50 km the small-scale eddies, although in some
77 literatures, they are often called sub-mesoscale eddies (Bassin et al., 2005; Burrage et
78 al., 2009).

79 The western SCS is one of the dynamically active regions in the SCS (Liu et al.,
80 2000). A northeastward alongshore current in summer (figure 1) and a southwestward
81 alongshore current in winter off the east coast of Vietnam are in accordance with wind
82 stress (Hwang and Chen, 2000; Morimoto et al., 2000; Yuan et al., 2005). The
83 northeastward alongshore current meanders off the southeastern coast of Vietnam and

84 leaves the Vietnam coast forming an eastward current driven by the southwest wind
 85 paralleled to the coast of eastern Vietnam (Hwang and Chen, 2000; Kuo et al., 2000;
 86 Barthel et al., 2009). The southwesterly monsoon and Ekman transport drive seasonal
 87 upwelling off southeastern Vietnam coast in summer, leading to more than 1°C drop
 88 in sea surface temperature (SST) (Wyrтки, 1961; Kuo et al., 2000; Metzger, 2003;
 89 Tang et al., 2006). A cold SST tongue around 12°N extends eastward. The orographic
 90 effect of coastal mountain ridge in the Vietnam can further intensify the southwesterly
 91 wind, and thus significantly enhances the coastal upwelling (Xie et al., 2003; Xie et
 92 al., 2007). The local orographic wind forces the coastal jet separation. This
 93 deformation and movement of coastal water induce mesoscale eddy activities (Gan et
 94 al., 2006; Wang et al., 2008; Chen et al., 2010). An eddy pair in the western SCS
 95 during upwelling season are generated probably due to the vorticity transports from
 96 the nonlinear effect of the western boundary currents (Xie et al., 2003; Ning et al.,
 97 2004; Wang et al., 2006; Chen et al., 2010). Moreover, a pair of anticyclonic eddies
 98 (A-A eddies pairs) in the western SCS during the upwelling season is mentioned by
 99 Kuo et al. (2000) and Xie et al. (2003).

100

101 **2. Data**

102 The study area locates in the western SCS, covering from 5°N-18°N,
 103 105°E-115°E (figure 1). The daily MERIS FR chlorophyll data from 2004 to 2009 are
 104 obtained from the European Space Agency (ESA). The daily 1 km
 105 Moderate-resolution Imaging Spectroradiometer (MODIS) SST data are obtained
 106 from National Aeronautics and Space Administration (NASA) Ocean Color project.

107 The mean sea level anomaly (MSLA) and geostrophic velocity data used here are
 108 extracted from the Delayed-Time Reference Series provided by Archiving, Validation
 109 and Interpretation of Satellite Data in Oceanography (AVISO). The mesoscale eddies
 110 are identified by a new SSH-based (sea surface height) method developed by Chelton
 111 et al. (2011). Rotational speed is computed by

$$112 \quad U = gf^{-1}A/L_s$$

113 Where g is the gravitational acceleration, f is the Coriolis parameter, A is the
 114 eddy amplitude (in centimetres) and L_s is the eddy length scale (in kilometres),
 115 defined by the radius of the circle that has the same area as the region within the
 116 closed contour of MSLA with maximum average geostrophic current speed (Chelton
 117 *et al.*, 2011).

118 The wind stress is obtained from the National Oceanic and Atmospheric
 119 Administration (NOAA) Environmental Research Division's Data Access Program
 120 (ERDDAP). The offshore transport (M_x) is calculated from

$$121 \quad M_x = \tau_y / f$$

122 Where τ_y is the wind stress parallel to the coastline, positive northward. It is
 123 replaced with the meridional direction wind stress since the most significant offshore

124 transport perpendicular to the Vietnam coast is approximately in the zonal direction.

125 **3. Results and discussion**

126 A series of small cyclonic phytoplankton tendrils at the southern edge of the
127 phytoplankton filament are found during June and October each year over 2004-2009
128 (figure 2). The phytoplankton tendrils have a mean diameter of 25 km and obviously
129 rotate out of the filament as the concentration variability of the phytoplankton tendril
130 seems consistent with the phytoplankton filament concentration variability. It is
131 implied that the phytoplankton tendril is rotated by the small-scale cyclonic eddy.
132 High levels of phytoplankton are frequently observed in the center of the small-scale
133 cyclonic eddies. The reason for this phenomenon will be discussed in the next section.

134 Figure 3 shows an evolution of two cyclonic phytoplankton tendrils during 9 July
135 2008 and 13 July 2008. It seems that these phytoplankton tendrils have a time scale of
136 several days. The phytoplankton tendril “A” is less obvious on 9 July 2008. Three
137 days later, the concentration of phytoplankton tendril “A” increases about 0.1 mg m^{-3} .
138 This high level of phytoplankton mainly occurs at the edge. The phytoplankton levels
139 in the center are relative low (approximately 0.07 mg m^{-3}). Only one day later, the
140 phytoplankton concentration in the center increases to approximately 0.3 mg m^{-3} and
141 becomes greater than the level of phytoplankton at the periphery. Another feature is
142 that the cyclonic “A” tends to propagate eastward. It propagates approximately 0.1°
143 ($\sim 10 \text{ km}$) from 12 July 2008 to 13 July 2008. The western boundary current has a
144 speed of about 12 cm s^{-1} (10.4 km d^{-1}) in the western SCS during summer (Cai et al.,
145 2007), which is consistent with the propagation velocity of the small cyclonic eddy
146 “A”. Therefore, the eastward propagating cyclonic eddy may be driven by the western
147 boundary current. The small cyclonic eddy B strengthens on 12 July 2008, with high
148 levels of phytoplankton within its interior. And then it disappears on 13 July 2008.

149 The observation of more detailed phytoplankton distribution in the tendrils is
150 attributed to the much finer resolution (300 m). We find that there are relative high
151 phytoplankton levels in the center of the small cyclonic eddies. One possible
152 mechanism is that the small cyclonic eddies keep rotating high phytoplankton and
153 perhaps nutrients, leading to the accumulation of phytoplankton in their center.
154 Another possible mechanism is that the vertical velocity of these small-scale cyclonic
155 eddies may drive episodic nutrient pulses to the euphotic zone to stimulate
156 phytoplankton growth (Lévy et al., 2012). Figure 4 shows the sea surface temperature
157 distribution associated with the phytoplankton tendril “A”. It is obvious that the cold
158 water is transported away from the cold tongue by the small-scale eddies. And the low
159 temperature water firstly occurs in the periphery of the eddies. Different from the
160 majority of mesoscale cyclonic eddy, there is not significant lower temperature water
161 in the center. It is implied that there is no upwelling or vertical mixing in the center.
162 Therefore, the phytoplankton distribution over this small-scale eddy may be
163 dominated by horizontal movement, and the relative high phytoplankton level in the
164 center of the cyclonic eddies “A” could be attributed to the accumulation of
165 phytoplankton or nutrients from the outer edge to interior under the rotation effect.

166 The small-scale eddies strengthen the horizontal diffusion of the nutrients and
167 phytoplankton (Capet et al., 2008a). These small cyclonic eddies are mainly observed
168 at the front of the filament, where strong differences in water mass properties result in
169 high strain rates and instabilities. Meanwhile, the small-scale eddies are also
170 associated with the occurrence of an anticyclonic mesoscale eddy to the south of the
171 filament (figure 3(a)). However, the small-scale cyclonic eddy does not occur for the
172 entire period of the offshore Ekman transport and the anticyclonic eddy. It only arises
173 at certain stages. We analyzed the offshore Ekman transport (M_x) and rotation speed
174 of the anticyclonic eddies during the development of the small-scale eddies over the
175 period of July 2008 shown in figure 3. Due to the limits of the cloud coverage and
176 satellite passing time, the image showing the declination of small-scale eddies is not
177 available. However, it is found that the small-scale eddies disappear on 22 July 2008.
178 Figure 3 (a) and (b) imply that the small-scale eddies may initially form on 9 July
179 2008. Therefore, we presumed that the small-scale eddies occur during the 9-22 July.
180 Figure 5 indicates that the offshore transport (M_x) decreases first and then increases
181 rapidly on 16 July. Different from the variability of M_x , the rotation speed increases
182 from 0.33 m s^{-1} on 2 July to 0.42 m s^{-1} on 12 July. And then it starts to decrease to
183 approximately 0.4 m s^{-1} on 16 July. At last, the rotation speed increases associated
184 with the strengthening of M_x . The variability of M_x seems not consistent with the
185 variability of the levels of phytoplankton (figure 3). The levels of phytoplankton has a
186 significant increases from 9 July to 13 July, accompanying with the decreases of the
187 M_x . This may be due to a lag between nutrients input and phytoplankton growth. The
188 normalized rotation speed of the anticyclonic eddy is defined as the ratio of the
189 rotation speed and the M_x , which indicates the relative movement between the
190 anticyclonic eddy and the offshore transport. The variability of the normalized
191 rotation speed shows that the small-scale eddies is associated with the greater relative
192 movement between the anticyclonic eddy and the offshore transport (figure 5). The
193 offshore current becomes meander under the influence of the anticyclonic eddy when
194 the offshore transport turns weaker and the rotation speed of the anticyclonic eddy
195 increases. The meandering current may stimulate the generation of the small-scale
196 process (Capet et al., 2008a, b).

197 The phytoplankton filament is consistent with the cold tongue induced by the
198 offshore Ekman transport, which is associated with negative sea surface height
199 anomaly relative to surround light and warm water. The small-scale eddies extend
200 from the cold tongue along the front. Therefore the heavy and cold water firstly
201 occurs in the periphery of small-scale eddies. Along the front, the transport from the
202 surface heavy water to the light water may be forced by the wind. Throughout the
203 development of the small-scale eddies, the wind direction exhibits some variations
204 (figure 6). Wind blowing varies from west-southwest (WSW) on 2 July 2008 (before
205 the generation of the small-scale eddies) to southwest (SW) on 9-13 July 2008 (during
206 the presence of the small-scale eddies). It implies that the small-scale eddies tend to
207 be associated with the more unidirectional uniform wind blowing along the
208 phytoplankton filament. Under spatially uniform wind forcing, the changed
209 meandering current may be more likely to generate the small-scale structure

210 (McGillicuddy et al., 2007; Mahadevan et al., 2008).

211 **4. Conclusion**

212 This paper describes the small-scale cyclonic eddies in the western SCS. Driven
213 by the small-scale cyclonic eddies, a series of phytoplankton tendrils occur at the
214 southern front of the wind-driven offshore current. These small-scale eddies have
215 horizontal scales less than 50 km and propagate eastward at the speed of 12 cm s^{-1} ,
216 accompanying with offshore current. Offshore current, the mesoscale anticyclonic
217 eddies and wind field may contribute to the generation of the small-scale cyclonic
218 eddies. Horizontal transport by the small-scale cyclonic eddies stimulates the
219 diffusion of the nutrients and phytoplankton of the western SCS.

220 **Acknowledgements**

221 We gratefully thank Ruixin Huang and Ian Jones for helpful comments and
222 suggestions. The MERIS 300 m chlorophyll data was provided by ESA-MOST
223 Dragon 3 Cooperation Programme from the European Space Agency. The sea surface
224 height and geostrophic current data were obtained from the Archiving Validation and
225 Interpretation of Satellite Data in Oceanography (AVISO). The MODIS sea surface
226 temperature was obtained from the NASA ocean color project. The wind stress is
227 obtained from the National Oceanic and Atmospheric Administration (NOAA)
228 Environmental Research Division's Data Access Program (ERDDAP). The research
229 was supported by the "Strategic Priority Research Program" of the Chinese Academy
230 of Sciences (No. XDA11010302), the Public science and technology research funds
231 projects of ocean (No. 201205040-6), the Innovation Group Program of State Key
232 Laboratory of Tropical Oceanography, South China Sea Institute of Oceanology,
233 Chinese Academy of Sciences (No. LTOZZ1201) and the National Natural Science
234 Foundation of China (No. 41006111).

235 **References**

- 236 Barthel, K., Rosland, R., and Thai, N.C.: Modelling the circulation on the continental
237 shelf of the province Khanh Hoa in Vietnam, *J. Marine Syst.*, 77(1-2), 89-113, 2009.
- 238 Bassion, C.J., Washburn, L., Brzezinski, M., and McPhee-Shaw, E.: Sub-mesoscale
239 coastal eddies observed by high frequency radar: A new mechanism for delivering
240 nutrients to kelp forests in the Southern California Bight, *Geophys. Res. Lett.*, 32,
241 L12604, 2005.
- 242 Bouffard, J., Renault, L., Ruiz, S., Pascual, A., Dufau, C., and Tintoré, J.: Sub-surface
243 small-scale eddy dynamics from multi-sensor observations and modeling, *Progr.*
244 *Oceanogr.*, 106, 62-79, 2012.
- 245 Burrage, D.M., Book, J.W., Martin, P.J.: Eddies and filaments of the Western Adriatic
246 Current near Cape Gargano: Analysis and prediction, *J. Marine Syst.*, 78, S205-S226,
247 2009.
- 248 Cai, S., Long, X., and Wang, S.: A model study of the summer Southeast Vietnam
249 Offshore Current in the southern South China Sea, *Cont. Shelf Res.*, 27, 2357-2372,
250 2007.

251 Capet, X., McWilliams, J.C., Molemaker, M.J., and Shchepetkin, A.F.: Mesoscale to
252 submesoscale transition in the California Current System. Part I: Flow structure, eddy
253 flux, and observational tests, *J. Phys. Oceanogr.*, 38, 29–43, 2008a.

254 Capet, X., McWilliams, J.C., Molemaker, M.J., and Shchepetkin, A.F.: Mesoscale to
255 submesoscale transition in the California Current System, Part II: Frontal processes. *J.*
256 *Phys. Oceanogr.*, 38, 44–64, 2008b.

257 Chelton, D.B., Schlax, M.G., and Samelson, R.M.: Global observations of nonlinear
258 mesoscale eddies, *Prog. Oceanogr.*, 91(2), 167-216, 2011.

259 Chen, G., Hou, Y., Zhang, Q., and Chu, X.: The eddy pair off eastern Vietnam:
260 Interannual variability and impact on thermohaline structure, *Cont. Shelf Res.*, 30(7),
261 715-723, 2010.

262 Gan, J., Li, H., Curchitser, E.N., and Haidvogel, D.B.: Modeling South China Sea
263 circulation: Response to seasonal forcing regimes, *J. Geophys. Res.*, 111(C6), C06034,
264 2006.

265 Genin, A., and Boehlert, G.W.: Dynamics of temperature and chlorophyll structures
266 above a seamount: An oceanic experiment, *J. Marine Syst.*, 43(4), 907-924, 1985.

267 Huang, B., Hu, J., Xu, H., Cao, Z., and Wang D.: Phytoplankton community at warm
268 eddies in the northern South China Sea in winter 2003/2004, *Deep-Sea Res. Pt. II*, 57,
269 1792-1798, 2010.

270 Hwang, C., and Chen S.-A.: Circulations and eddies over the South China Sea derived
271 from TOPEX/Poseidon altimetry, *J. Geophys. Res.*, 105(C10), 23943-23965, 2000.

272 Kuo, N.-J., Zheng, Q., and Ho, C.-R.: Satellite Observation of Upwelling along the
273 Western Coast of the South China Sea, *Remote Sens. Environ.*, 74(3), 463-470, 2000.

274 Lévy, M., Ferrari, R., Franks, P.J.S., Martin, A.P., and Rivière, P.: Bringing physics
275 to life at the submesoscale, *Geophys. Res. Lett.*, 39, L14602, 2012.

276 Liu, Y., Weisberg, R.H., and Yuan, Y.: Patterns of upper layer circulation variability
277 in the South China Sea from satellite altimetry using the Self-Organizing Map, *Acta*
278 *Oceanol. Sin.*, 27(Supp.), 129-144, 2008.

279 Liu, Y., Yuan, Y., Su, J., and Jiang, J.: Circulation in the South China Sea in summer
280 of 1998, *Chinese Sci. Bull.*, 45(18), 1648-1655, 2000.

281 Mahadevan, A., Thomas, L.N., and Tandon, A.: Comment on "eddy/wind interactions
282 stimulate extraordinary mid-ocean plankton blooms", *Science*, 320, 448, 2008.

283 McGillicuddy, D.J., Anderson, L.A., Bates, N.R., Bibby, T., Buesseler, K.O., Carlson,
284 C.A., Davis, C.S., Ewart, C., Falkowski, P.G., Goldthwait, S.A., Hansell, D.A.,
285 Jenkins, W.J., Johnson, R., Kosnyrev, V.K., Ledwell, J.R., Li, Q.P., Siegel, D.A., and
286 Steinberg, D.K.: Eddy/wind interactions stimulate extraordinary mid-ocean plankton
287 blooms, *Science*, 316, 1021-1026, 2007.

288 Metzger, E.: Upper Ocean Sensitivity to Wind Forcing in the South China Sea, *J.*
289 *Oceanogr.*, 59(6), 783-798, 2003.

290 Morimoto, A., Yoshimoto, K., and Yanagi, T.: Characteristics of sea surface
291 circulation and eddy field in the South China Sea revealed by satellite altimetric data,
292 *J. Oceanogr.*, 3, 331-344, 2000.

293 Nicholson, S.: Linking small-scale circulation dynamics with large-scale seasonal
294 production (phytoplankton) in the Southern Ocean, 4th CSIR Biennial Conference:

295 Real problems relevant solutions, CSIR, Pretoria, 9-10 October 2012
296 Ning, X., Chai, F., Xue, H., Cai, Y., Liu, C., and Shi, J.: Physical-biological
297 oceanographic coupling influencing phytoplankton and primary production in the
298 South China Sea, *J. Geophys. Res.*, 109(C10), C10005, 2004.
299 Pegau, W., Boss, E., and Martínez, A.: Ocean color observations of eddies during the
300 summer in the Gulf of California, *Geophys. Res. Lett.*, 29(9), 1-3, 2002.
301 Tang, D.L., Kawamura, H., Shi, P., Takahashi, W., Guan, L., Shimada, T., Sakaida, F.,
302 and Isoguchi, O.: Seasonal phytoplankton blooms associated with monsoonal
303 influences and coastal environments in the sea areas either side of the Indochina
304 Peninsula, *J. Geophys. Res.*, 111(G1), G01010, 2006.
305 Tang, D., Kawamura, H., Dien, T., and Lee, M.: Offshore phytoplankton biomass
306 increase and its oceanographic causes in the South China Sea, *Mar. Ecol. Prog. Ser.*
307 268, 31-41, 2004.
308 Wang, G., Chen, D., and Su, J.: Generation and life cycle of the dipole in the South
309 China Sea summer circulation, *J. Geophys. Res.*, 111(C6), C06002, 2006.
310 Wang, G., Chen, D., and Su, J.: Winter Eddy Genesis in the Eastern South China Sea
311 due to Orographic Wind Jets, *J. Phy. Oceanogr.*, 38(3), 726-732, 2008.
312 Wyrтки, K.: Physical Oceanography of the Southeast Asian waters, NAGA Rep. 2,
313 195 pp., Scripps Inst. Oceanogr, La Jolla, Calif, 1961.
314 Xie, S.-P., Xie, Q., Wang, D., and Liu, W.T.: Summer upwelling in the South China
315 Sea and its role in regional climate variations, *J. Geophys. Res.*, 108(C8), 3261, 2003.
316 Xie, S.-P., Chang, C.-H., Xie, Q., and Wang D.: Intraseasonal variability in the
317 summer South China Sea: Wind jet, cold filament, and recirculations, *J. Geophys.*
318 *Res.*, 112(C10), C10008, 2007.
319 Xiu, P., and Chai, F.: Modeled biogeochemical responses to mesoscale eddies in the
320 South China Sea, *J. Geophys. Res.*, 116(C10), C10006, 2011.
321 Yuan, Y., Liu, Y., Liao, G., Lou, R., Su, J., and Wang, K.: Calculation of circulation in
322 the South China Sea during summer of 2000 by the modified inverse method, *Acta*
323 *Oceanol. Sin.*, 24(1), 14-30, 2005.

324 Figure captions

325 Figure 1. (a) Bathymetry of the South China Sea (Unit: m), the red rectangle
326 represents the study area. (b) Mean surface geostrophic currents in June-October of
327 2002-2008.

328

329 Figure 2. Daily 300 m MERIS chlorophyll (unit: mg m^{-3}) on (a)-(b) 5 September 2004,
330 (c)-(d) 22 June 2005, (e)-(f) 7 June 2006, (g)-(h) 21 July 2007, (i)-(j) 16 July 2008,
331 (k)-(l) 29 July 2009. The cloud covered area is masked by the white color.

332

333 Figure 3. Daily 300 m MERIS chlorophyll (unit: mg m^{-3}) on (a) 9 July 2008, (b) 12
334 July 2008, (c) 13 July 2008. The cloud covered area is masked by the white color. 'A'
335 and 'B' indicate two small cyclonic eddies respectively. The pink circle in (a) denotes
336 the anticyclonic mesoscale eddy (AME) on 9 July 2008, which is derived from
337 AVISO MSLA data following the method of Chelton et al. (2011).

338

339 Figure 4. MODIS 1 km sea surface temperature distribution (unit: $^{\circ}\text{C}$) on 13 July
340 2008.

341

342

343 Figure 5. The offshore transport (M_x , $\text{kg m}^{-1} \text{s}^{-1}$), rotation speed of the mesoscale
344 anticyclonic eddy (U , cm s^{-1}) and the normalized rotation speed to M_x (U/M_x),
345 indicating the relative importance of the mesoscale anticyclonic eddy and offshore
346 Ekman transport in the form of small-scale eddies.

347

348 Figure 6. Wind field on 2 July 2008 (the blue arrow), 12 July 2008 (the red arrow)
349 and 26 July 2008 (the green arrow).

350

351

352

353

354

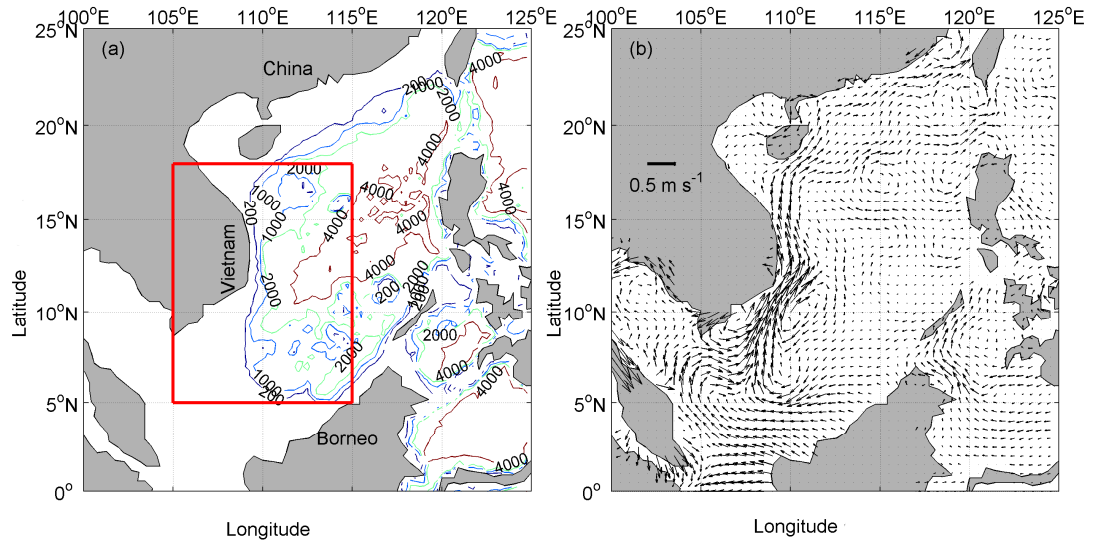
355

356

357

358 Figures

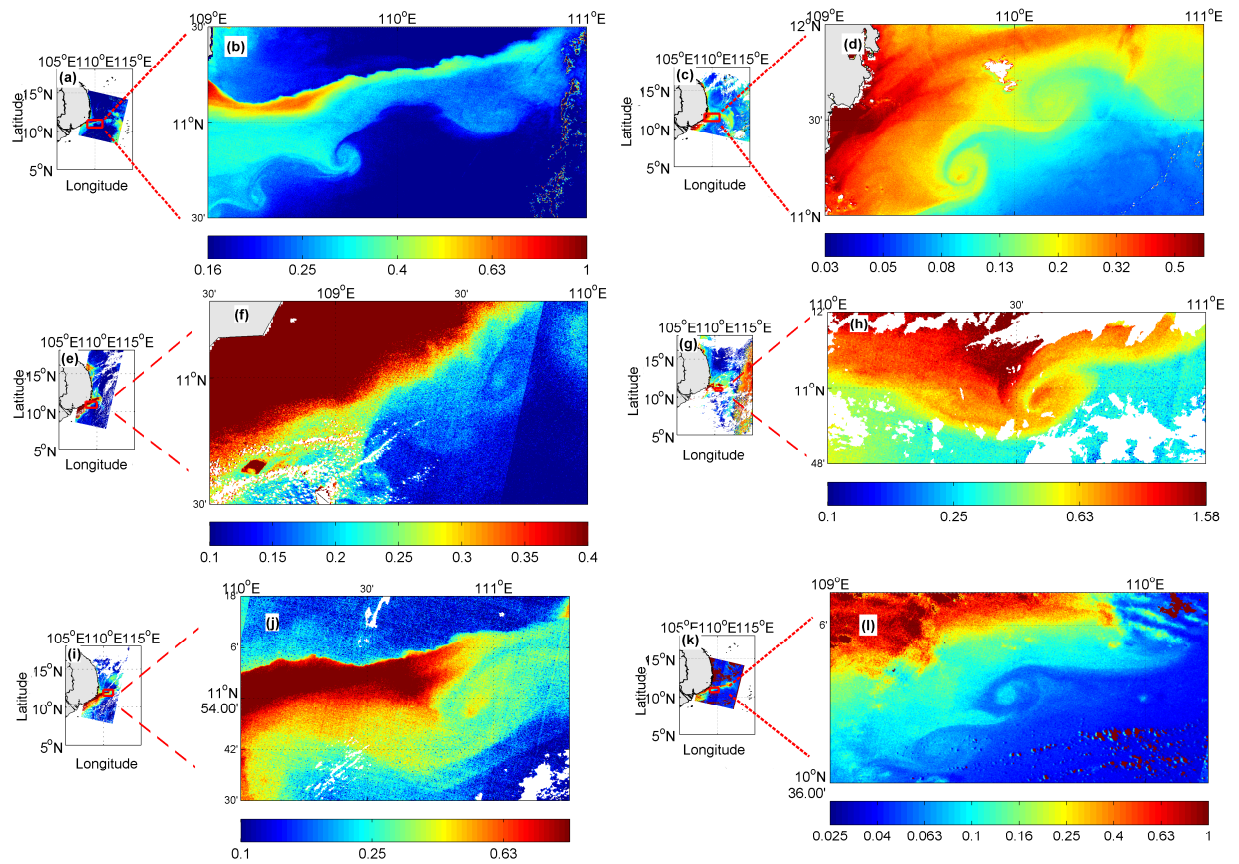
359 Figure 1



360

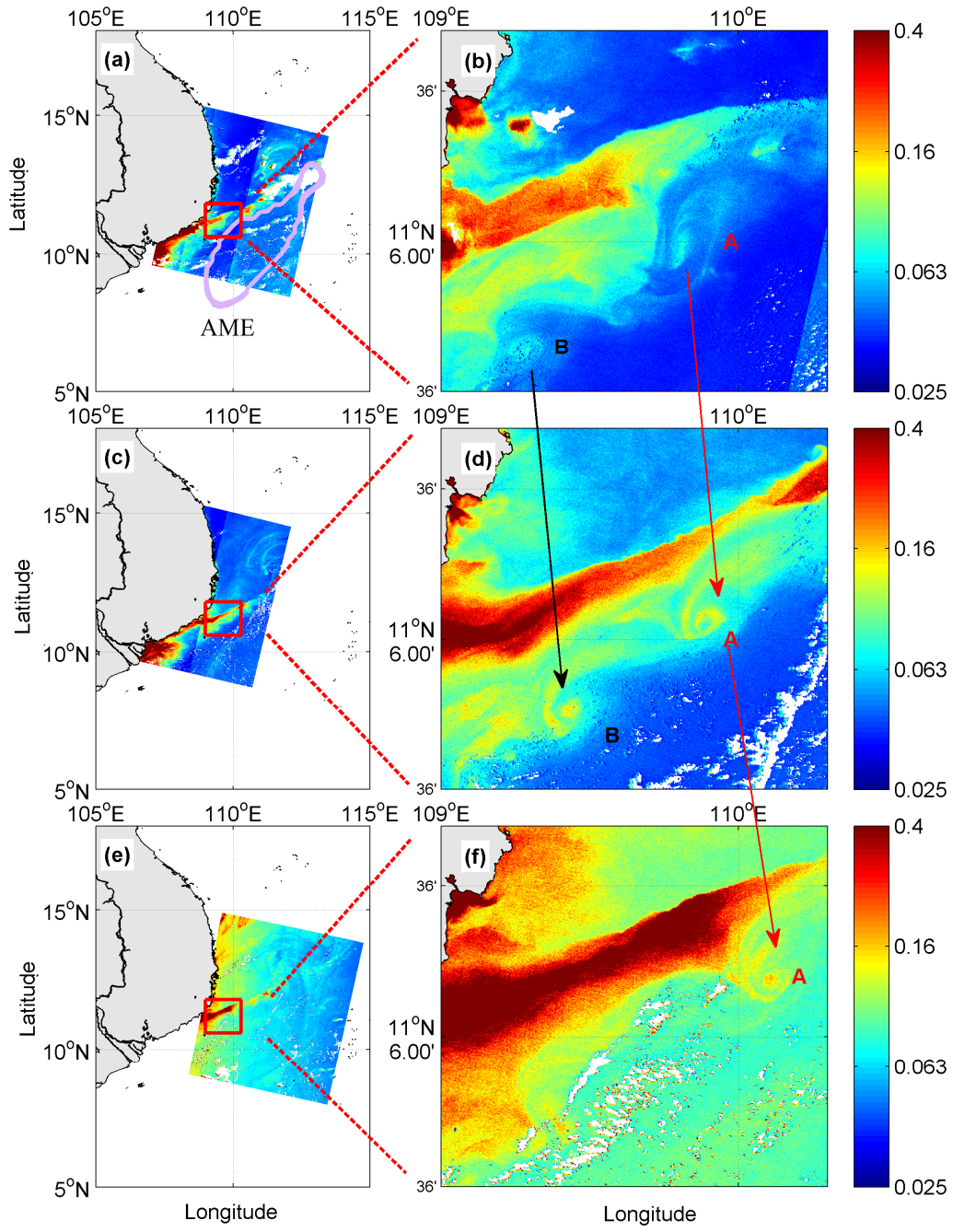
361

362 Figure 2



363

364 Figure 3



365

366

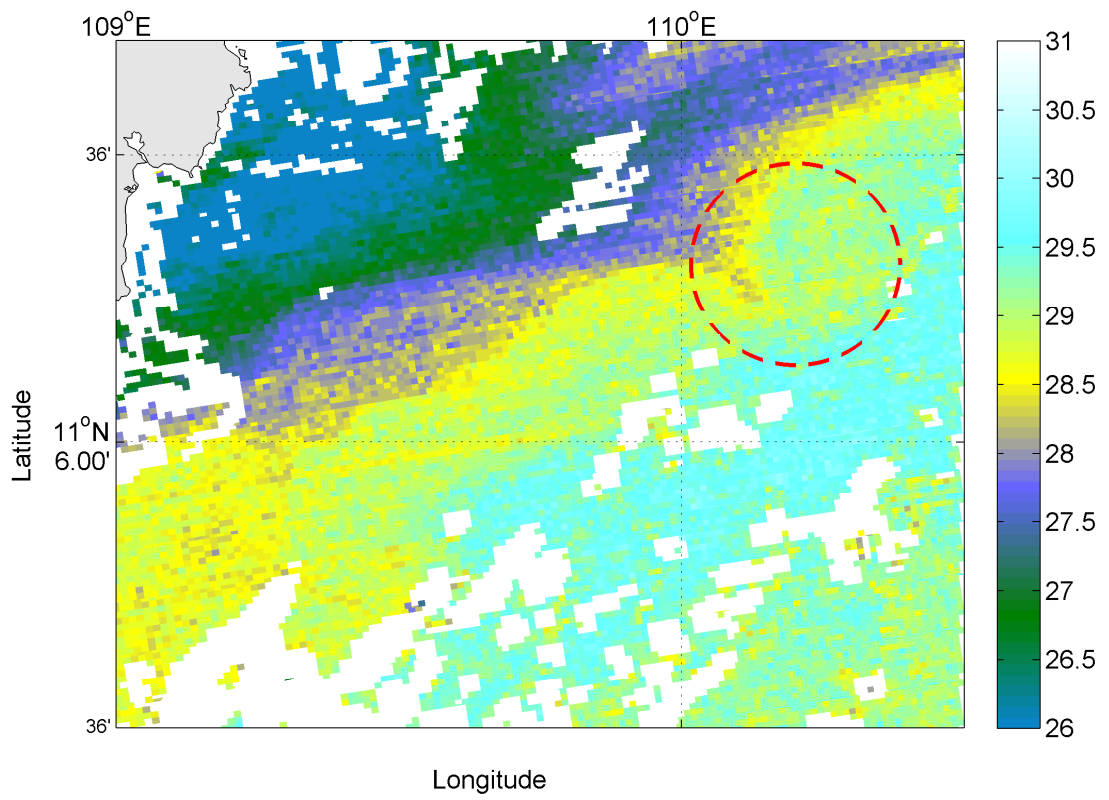
367

368

369

370

371 Figure 4



372

373

374

375

376

377

378

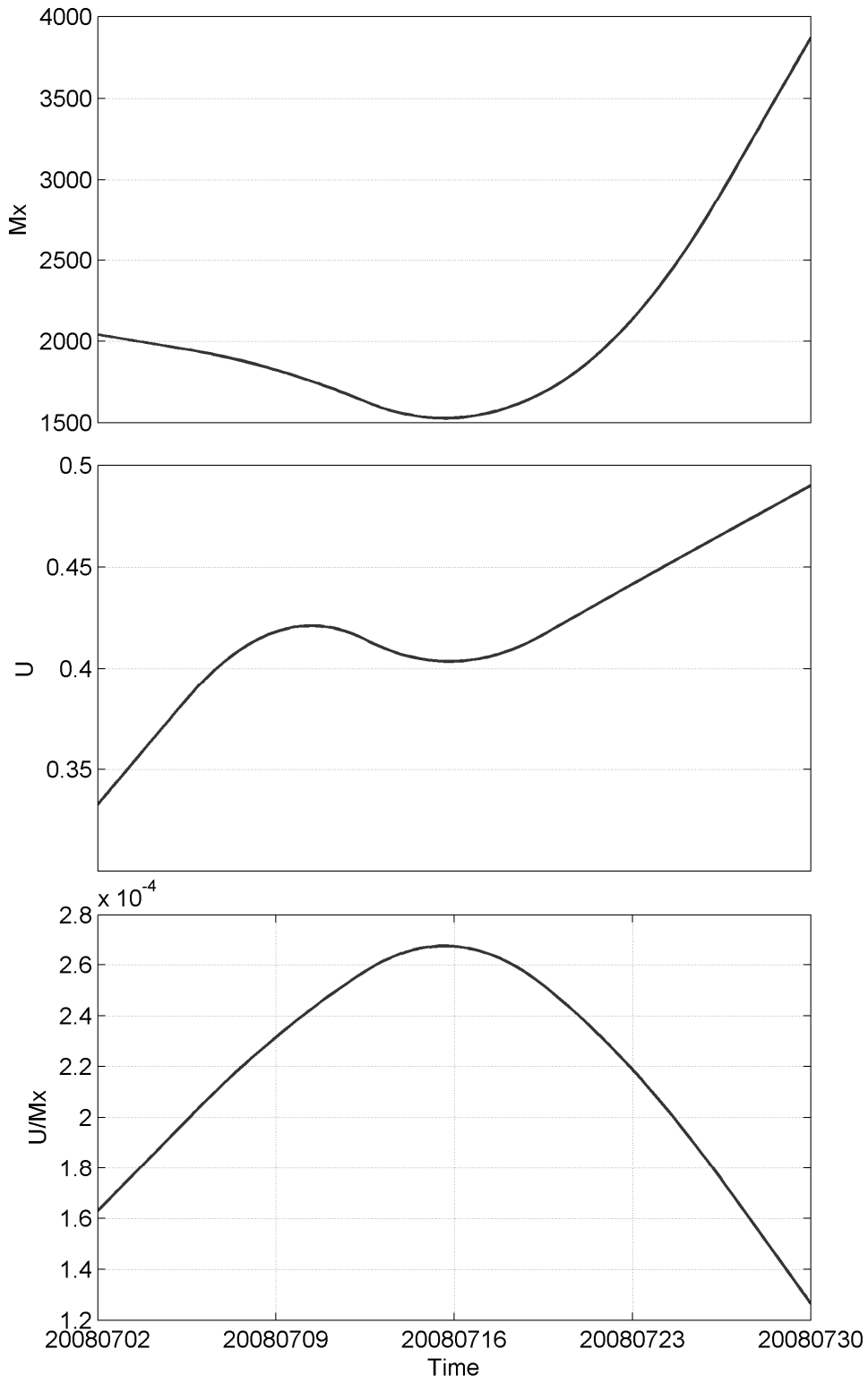
379

380

381

382

383 Figure 5

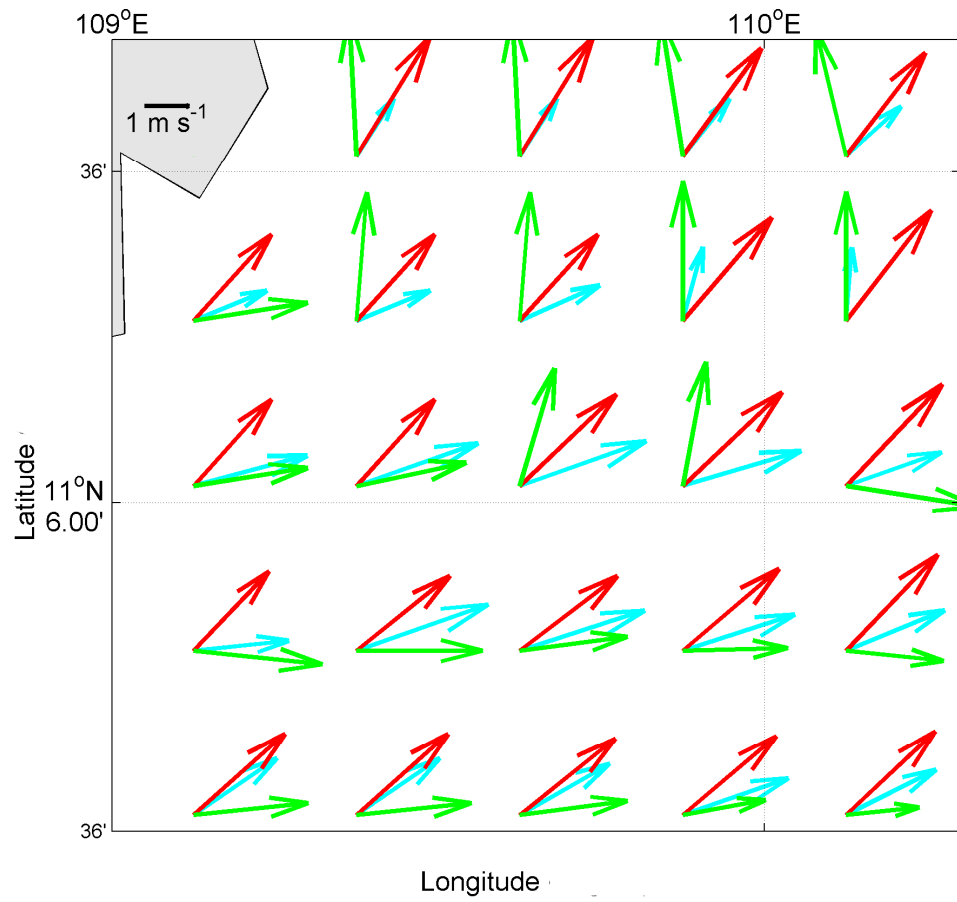


384

385

386

387 Figure 6



388

389

390